Bulletin of the Seismological Society of America, Vol. 88, No. 6, pp. 1379–1391, December 1998

Faulting Apparently Related to the 1994 Northridge, California, Earthquake and Possible Co-seismic Origin of Surface Cracks in Potrero Canyon, Los Angeles County, California

by R. D. Catchings, M. R. Goldman, W. H. K. Lee, M. J. Rymer, and D. J. Ponti

Abstract Apparent southward-dipping, reverse-fault zones are imaged to depths of about 1.5 km beneath Potrero Canyon, Los Angeles County, California. Based on their orientation and projection to the surface, we suggest that the imaged fault zones are extensions of the Oak Ridge fault. Geologic mapping by others and correlations with seismicity studies suggest that the Oak Ridge fault is the causative fault of the 17 January 1994 Northridge earthquake (Northridge fault). Our seismically imaged faults may be among several faults that collectively comprise the Northridge thrust fault system. Unusually strong shaking in Potrero Canyon during the Northridge earthquake may have resulted from focusing of seismic energy or co-seismic movement along existing, related shallow-depth faults. The strong shaking produced ground-surface cracks and sand blows distributed along the length of the canyon. Seismic reflection and refraction images show that shallow-depth faults may underlie some of the observed surface cracks. The relationship between observed surface cracks and imaged faults indicates that some of the surface cracks may have developed from nontectonic alluvial movement, but others may be fault related. Immediately beneath the surface cracks, *P*-wave velocities are unusually low (<400 m/sec), and there are velocity anomalies consistent with a seismic reflection image of shallow faulting to depths of at least 100 m. On the basis of velocity data, we suggest that unconsolidated soils (<800 m/sec) extend to depths of about 15 to 20 m beneath our datum (<25 m below ground surface). The underlying rocks range in velocity from about 1000 to 5000 m/sec in the upper 100 m. This study illustrates the utility of high-resolution seismic imaging in assessing local and regional seismic hazards.

Introduction

Potrero Canyon, Los Angeles County, California, is located about 35 km northwest of the city of Los Angeles (Figs. 1 and 2) and is one of four areas that experienced major surface cracking during the 17 January 1994 (M_w 6.7) Northridge earthquake (Hart *et al.,* 1995; Hecker *et al.,* 1995; Rymer *et al.,* 1995). As a result of strong shaking during the Northridge earthquake, extensional cracks occurred along both sides of Potrero Canyon, but compressional surface deformation (surficial thrust faults and cracks) occurred along the south side of the canyon (Rymer *et al.,* 1995) (Fig. 3). The concentration of shallow (~1 m) compressional cracks on the south was initially thought to represent possible co-seismic rupture. Subsequent detailed geologic investigations of the cracks led Rymer *et al.* (1995) to conclude that the cracks resulted from nontectonic alluvial movement caused by gravity. However, Shen *et al.* (1996) and Hudnut *et al.* (1996) suggest that geodetic measurements are consistent with co-seismic faulting in the general area that includes Potrero Canyon. Furthermore, the mainshock of the Northridge earthquake, located approximately 22 km south-southeast of Potrero Canyon, occurred on a south-dipping blind thrust fault that projects toward the ground surface near Potrero Canyon (U.S. Geological Survey and Southern California Earthquake Center, 1994; Hauksson *et al.,* 1995). Seismicity immediately preceding, during, and after the Northridge earthquake roughly defines an area of deformation that terminates in the vicinity of Potrero Canyon (Hauksson *et al.,* 1995; Pujol, 1996).

The observed surface cracking, liquefaction, and strong shaking (L. Wennerberg, personal comm., 1994; Wald *et al.,* 1996) in Potrero Canyon near the surface projection of the Northridge fault prompted the U.S. Geological Survey to conduct a series of investigations there, including paleoseismological trenching (Rymer *et al.,* 1995), borings, and cone

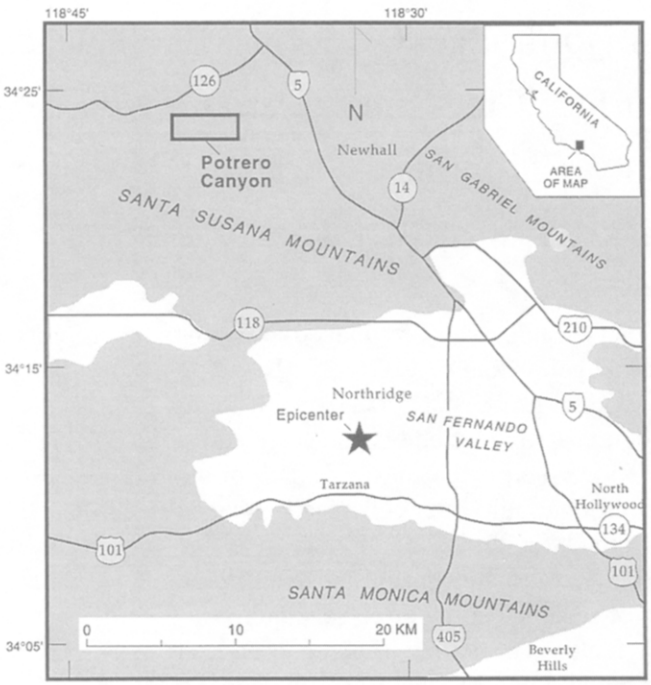

Figure 1. Location map of the northern Los Angeles County area with major highways. The star shows the epicenter of the 17 January 1994 Northridge earthquake relative to Potrero Canyon (box). The white shading shows major sedimentary basins. The inset shows the study (black box) areas within the state of California.

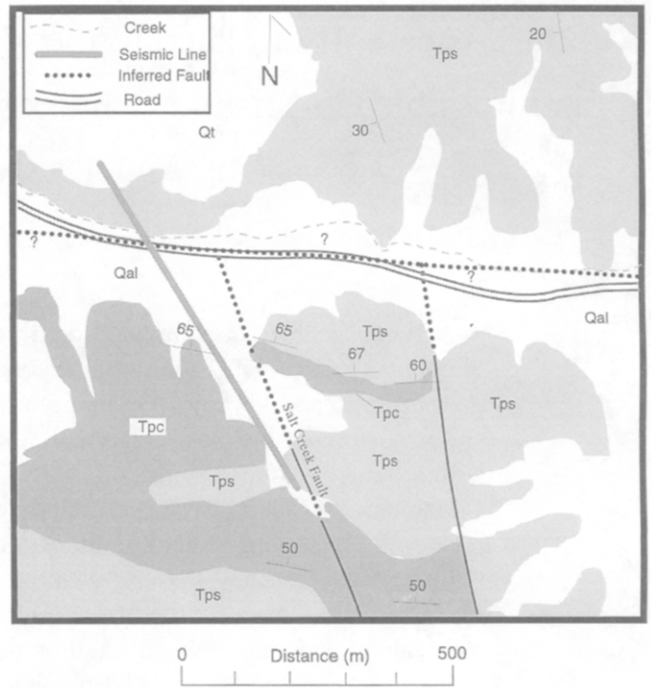

Figure 2. Geologic map (from Winterer and Durham, 1962) of the western part of Potrero Canyon in the vicinity of our seismic profile. On the basis of geologic mapping, Winterer and Durham suggest two faults near our seismic profile: an axial fault within the valley and the Salt Creek fault subparallel to our seismic profile. Strikes and dips (numbers in degrees) of strata are shown. Qal, Qt, Tpc, and Tps refer to Quaternary alluvium, Quaternary terrace deposits, Pliocene Pico Formation conglomerates, and siltstones, respectively.

penetration tests (Holzer *et al.,* 1996). These investigations were conducted across the surface cracks to look for evidence of shallow seismogenic faulting; none was found. To look for deeper (>3 m) expressions of faulting, we conducted a seismic reflection and refraction survey across Potrero Canyon centered on the trenches. In this report, we present seismic reflection images of apparent shallow (<100 m) faulting, the associated *P*-wave velocity structure, and a deeper image (to 1.5 km depth) of faulting that may be part of a system of faults that constitutes the causative fault of the Northridge earthquake (referred to here as the Northridge fault).

Geological Setting

Potrero Canyon is located north of the Santa Susana mountains and trends approximately east–west for less than 5 km (Fig. 1). Near our seismic line, the valley floor is about 200 m wide but varies in width along the length of the canyon (Figs. 2 and 3). Potrero Canyon is one of a series of east–west-trending valleys within the Transverse Ranges of southern California that have undergone late Cenozoic faulting and folding (Wentworth and Yerkes, 1971). A number of thrust faults have been mapped to the south, north, and west of Potrero Canyon (Winterer and Durham, 1962; Yeats *et al.,* 1994), and deep well logs infer other buried thrust faults to the east. The nearby faults are both north dipping and south dipping, and the strikes of these faults vary greatly.

Potrero Canyon is believed to be within or overlie a syncline that is faulted along its axis (Winterer and Durham, 1962; see Fig. 2). On the south side, the basement and canyon walls in the immediate vicinity of our seismic line are north dipping (50° to 70°), and on the north side, they are southwest dipping (20° to 50°). The exposed rocks consist of sandstone, conglomerate, and mudstone of the Pliocene Pico Formation (Winterer and Durham, 1962). Surface exposures of bedrock and associated faults and folds in Potrero Canyon indicate that structures vary greatly over relatively short distances, ranging from steeply dipping strata on fold limbs to nearly subhorizontal layers. Within Potrero Canyon, surface and near-surface sediment types consist of a series of Holocene sand, gravel, and clay loam within the upper few meters (Rymer *et al.,* 1995; Holzer *et al.,* 1996).

Seismic Data Acquisition

In February 1994, we acquired an approximately northwest–southeast-trending, 700-m-long, combined seismic re-

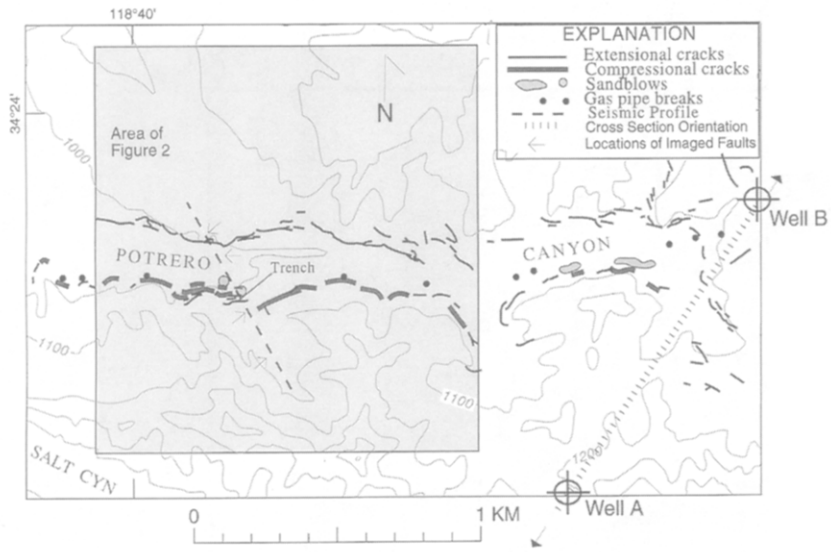

Figure 3. Topographic map of Potrero Canyon with the locations of surface cracks, a trench, and sand blows (from Rymer *et al.*, 1995) relative to our seismic profile. The box outlines the area of the geologic map of Figure 2, and the hachured line shows the approximate location of cross section E-E′ of Winterer and Durham (1962). Deep oil wells (A and B) are shown.

flection and refraction survey across Potrero Canyon (Fig. 2). Seismic sources consisted of 1-lb. charges of ammonium nitrate in approximately 2-m-deep holes. Seismic sources were detonated approximately every 15 m along the southern 500 m of the seismic array, but sources were not located along the northern 150 m of the seismic array because shot holes could not be drilled on the steeper topography. The seismic data were recorded on 46 channels of a PC-based recording system (Lee, 1989; Lee and Dodge, 1992). Sensors consisted of 46 strings of six 8-Hz, Mark Products geophones spaced 15 m apart and connected by cable. The seismic data were recorded using a 2-msec sampling interval without filters. Each shot point was colocated with a sensor to determine the shot time. Elevation and relative locations were determined using an electronic distance meter with a precision of about 1 mm. Details of the acquisition parameters are described in Jaasma *et al.* (1997). Five-second records were recorded on the PC hardisk in PC-SUDS format (Lee, 1989) for each shot. The seismic data were then transferred to optical disk for permanent storage.

Velocity Modeling Approach

The data were processed using both seismic refraction and seismic reflection techniques. Using these two approaches on the same data provides independent constraints on the subsurface. In seismic refraction processing, the first arrivals were measured, and a starting model was developed based on calculated velocities and travel times. The starting model was then input into a modified version of a velocity inversion routine developed by Hole (1992). This method effectively measures the travel time through each section of the velocity model and compares the calculated travel times with the observed travel times. The inversion routine modifies the velocity structure in successive iterations on the basis of misfits among calculated and observed travel times until an acceptable fit is achieved.

Our final velocity model is shown in Figure 4a, and a lithologic interpretation of the velocity model is shown in Figure 4b. Seismic velocities were measured from the surface to a maximum depth of approximately 150 m and laterally from about meter 25 to about meter 675 of the velocity model (Fig. 4). The maximum depth of penetration of refracted seismic energy is a function of the velocity gradients within the Earth and the length of the seismic recording array. Because our seismic array was limited to about 700 m in length, the depth of penetration of refracted arrivals was limited to less than ~130 m.

The resolution of any part of the velocity model depends on the number of ray paths that transverse through that part of the velocity model. Where there are many separate ray paths through a given part of the velocity model, the calculated velocity structure is likely to be well resolved and reasonably accurate. Because a total of 31 shots were located along the seismic profile, parts of the velocity model have more than 75 separate ray paths through it. Near the ends of the seismic profile, however, parts of the velocity model have less than 5 separate ray paths. Thus, we expect the velocity model to be most accurate between meters 50 and 650.

Velocities range from less than 300 m/sec at the surface to about 5 km/sec at approximately 130 m depth. Within the upper 50 m, there is a high-velocity gradient, whereby velocities increase from less than 300 m/sec to more than 3000 m/sec. At the surface, the low velocities (≦400 m/s) occur near meters 277, 375, and 550 (Fig. 4a).

Reflection Imaging Approach

The seismic reflection data are presented as stacked, migrated sections. Depths on the reflection sections are relative

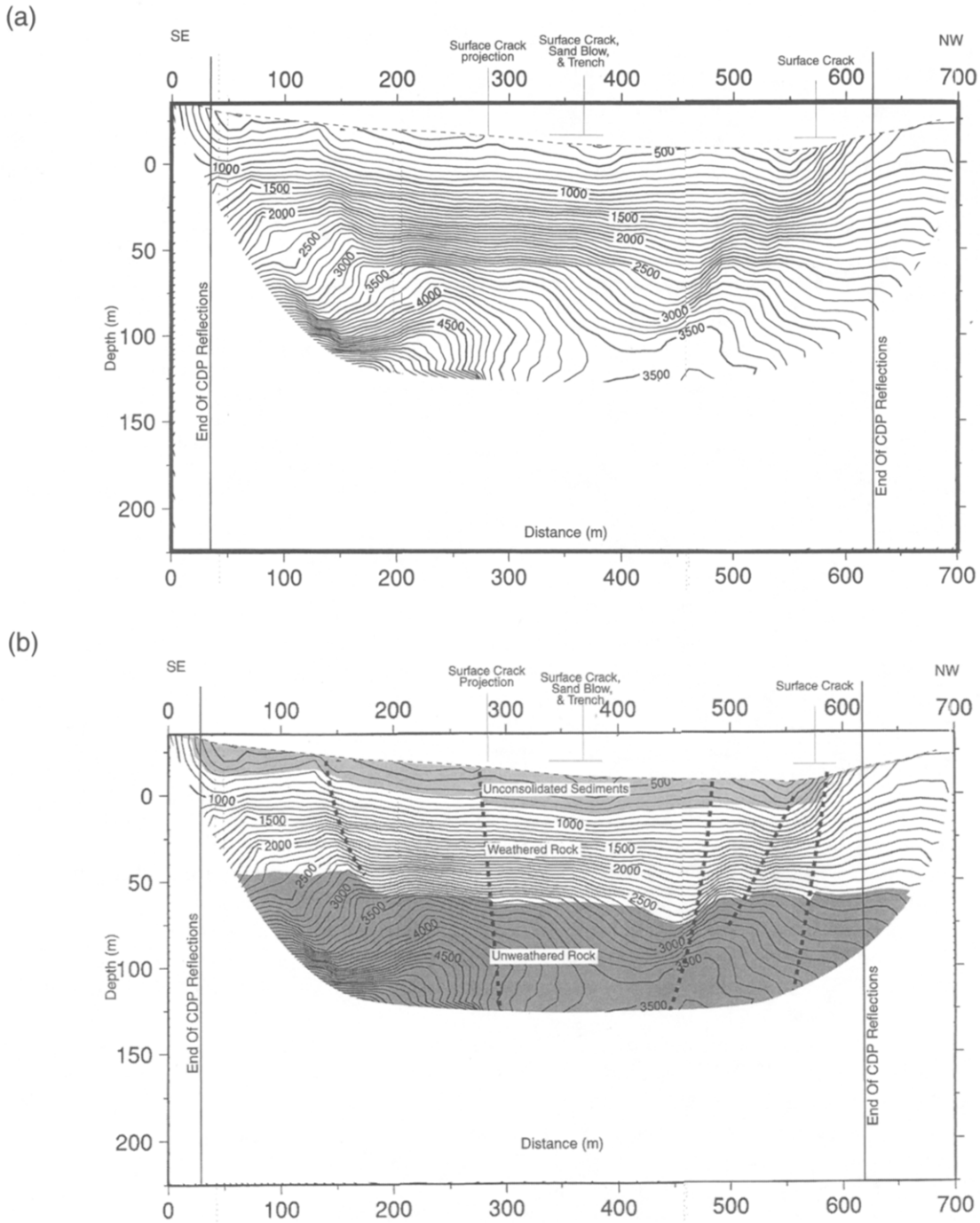

Figure 4. (a) Seismic *P*-wave velocity model derived from inversion of first arrivals of the seismic data. Contours are velocities in meters per second. Depth and distance are in meters. Depth is relative to the topographically lowest point along the seismic profile. The locations of nearby surface cracks, sand blows, and a paleoseismological trench are shown along the top. The area of the CDP reflection profile of Figure 5 is outlined by the vertical lines. (b) The same velocity model as (a) with interpretative faults (dashed lines) and basic lithologic units.

to a datum set at our topographically lowest geophone, which was about 4.5 m lower than the trench of Rymer *et al.* (1995). The final velocities used in stacking the near-surface data were derived from the inverted first arrivals for the upper 100 m of the section. Below 100 m, we used standard reflection velocity analysis (semblance) to determine velocities. Because the greatest variations in velocity are typically in the near surface, the increased accuracy from the velocity data allowed for an improved stack. The seismic reflection data processing sequence included geometry in-

stallation, trace editing, frequency filtering, muting, AGC, velocity determination, elevation statics, stacking, and migration.

Stacked seismic reflection images include the depth ranges from about 4 m (Figs. 5a and 5b) to about 1.5 km (Figs. 6a and 6b) below the surface. For reference with the velocity model, seismic reflections image the subsurface with common depth points from about meter 22 to meter 617 of the velocity model.

The resolution of the seismic reflection images depend on the frequencies recorded, the shot spacing, and the sensor spacing. Most of our seismic reflection data range from about 20 to 150 Hz. For the deeper subsurface with velocities of approximately 5000 m/sec, only reflectors that are about 10 m thick or more would produce reflections. For the shallower section with velocities of approximately 500 m/sec, reflectors on the order of 1 m or more thick should produce reflections; however, it is unlikely that we can follow 1-m-thick layers laterally for appreciable distances because of our sensor and shot spacing. Most of the layers imaged in the upper few hundred meters appear to be a minimum of about 2 to 5 m thick (Fig. 5), and those in the deeper sections appear to be about 10 m thick (Fig. 6).

Interpretation

Shallow Subsurface

On the basis of seismic refraction velocities and depth to reflecting boundaries, we interpret the thickness of unconsolidated sediments to be about 15 to 20 m (relative to our datum, rtd; see previous section for datum) in Potrero Canyon (Figs. 4b and 5b). Seismic refraction velocities are reliable in differentiating between sediments and rock because we have velocity data on the hills (sedimentary rock) and within the valley (unconsolidated sediments). The surficial sedimentary rocks that constitute the surrounding hills have *P*-wave velocities ranging from about 800 m/sec to about 1200 m/sec, and in the valley where there are surficial unconsolidated sediments, *P*-wave velocities are less than 800 m/sec. From about meter 150 to about meter 600 of the velocity model (Fig. 4), *P*-wave velocities less than 800 m/sec extend from the surface to depths of about 15 to 20 m rtd, below which velocity contours become more closely spaced, signaling a change in physical properties.

The ~15 to 20 m (rtd) depth to consolidated rock beneath the valley is also consistent with seismic reflection data (Fig. 5). A coherent reflection varies laterally from about 17 to 23 m (rtd) depth beneath the valley, suggesting a velocity contrast that is consistent with a transition from unconsolidated sediments (~800 m/sec) to more consolidated rock (800 to 3000 m/sec). Holzer *et al.* (1996) also found from cone penetration tests that the unconsolidated sediments were at least 15 m deep in Potrero Canyon.

Within the unconsolidated sediments, there are three locations with low (<400 m/sec) *P*-wave velocities (near meters 200 to 280, 350 to 400, and 520 to 580). These low-velocity areas occur near the locations of surface cracks or at the westward projection of a surface crack; however, the low-velocity anomaly near meter 375 also occurs at the surface location of a sand blow. We interpret all of the low-velocity areas as resulting from lesser consolidated sediments relative to those sediments along other areas of the seismic profile. Sand blows or open cracks, such as those generated by earthquake-induced shaking, may account for the low velocities, but we cannot determine whether those low velocities existed prior to the development of the sand blows or cracks. We are aware of no other reports of *P*-wave velocities as low as these for the region. For example, seismic-refraction-determined *P*-wave velocities for an area south of the Northridge earthquake epicenter is about three times as high (950 m/sec) for the shallow subsurface (Catchings and Lee, 1996), and at 19 different locations throughout the Los Angeles area, Fumal *et al.* (1981) found near-surface *P*-wave velocities in boreholes to be well above 500 m/sec.

Abrupt deflections in the velocity contours and lower velocities have been shown to correspond to faults elsewhere (Jarchow *et al.,* 1994; Lutter *et al.,* 1994). The observed deflections in the velocity contours beneath some of the surface cracks are consistent with ground breakage or faults that extend to the deeper (at least 100 m) subsurface. The low-velocity areas near the northwesternmost surface cracks (meter 550 to 590) and the westward projection of the southernmost surface crack (see Fig. 3 and meter 277 of Fig. 4b) are consistent with apparent faulting observed in the seismic reflection sections to depths of approximately 100 m (Figs. 5a and 5b). However, the low-velocity area at meter 375 of the velocity model (at the trench) does not appear to be fault related, as no fault was observed in either the trench (Rymer *et al.,* 1995) or the seismic section (Fig. 5b) at that location. Due to the proximity of a nearby sand blow and lack of an imaged fault, it is likely that the near-surface low-velocity feature observed at meter 375 is related to shaking-induced deformation (Fig. 3). Conversely, the apparent fault located at meter 480 of the seismic reflection section (Fig. 5b) does not show evidence of surface cracking, but this apparent fault is consistent with the location of an axial fault inferred by Winterer and Durham (1962) on the basis of geologic mapping (Fig. 2).

We agree with Rymer *et al.*'s (1995) assessment that the surface cracks near the trench (meter 375) resulted from gravity-induced alluvial movement caused by strong shaking because (1) the physical conditions at meter 375 were sufficient to generate sand blows (Holzer *et al.,* 1996) and (2) we observe no evidence for faulting at meter 375 from seismic imaging. At meters 277 and 595, however, we suggest that colocated surface cracks, seismically imaged faults, and deep (~100 m) velocity anomalies are indicative of subsurface faulting. The faults at meters 277 and 595 are probably structures that existed prior to the Northridge earthquake. We can make no determination of whether there was movement on these shallow faults during the Northridge earth-

(a)

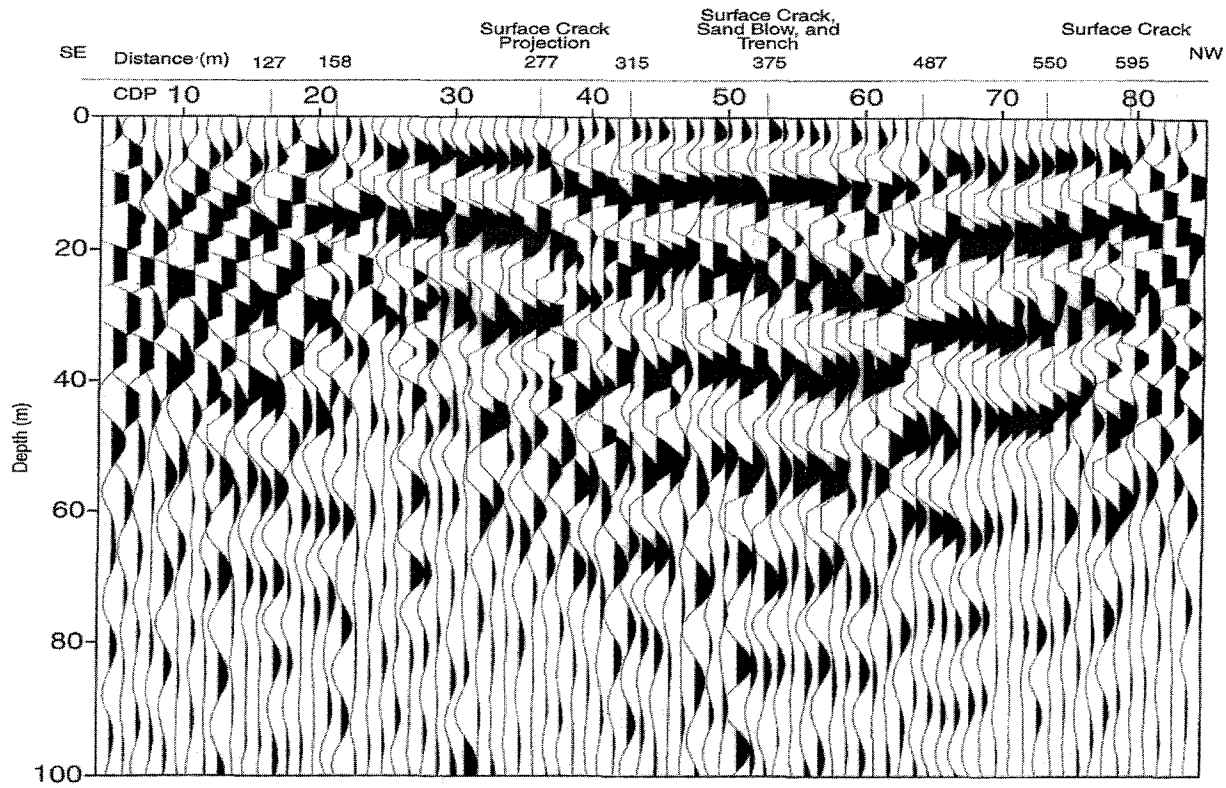

(b)

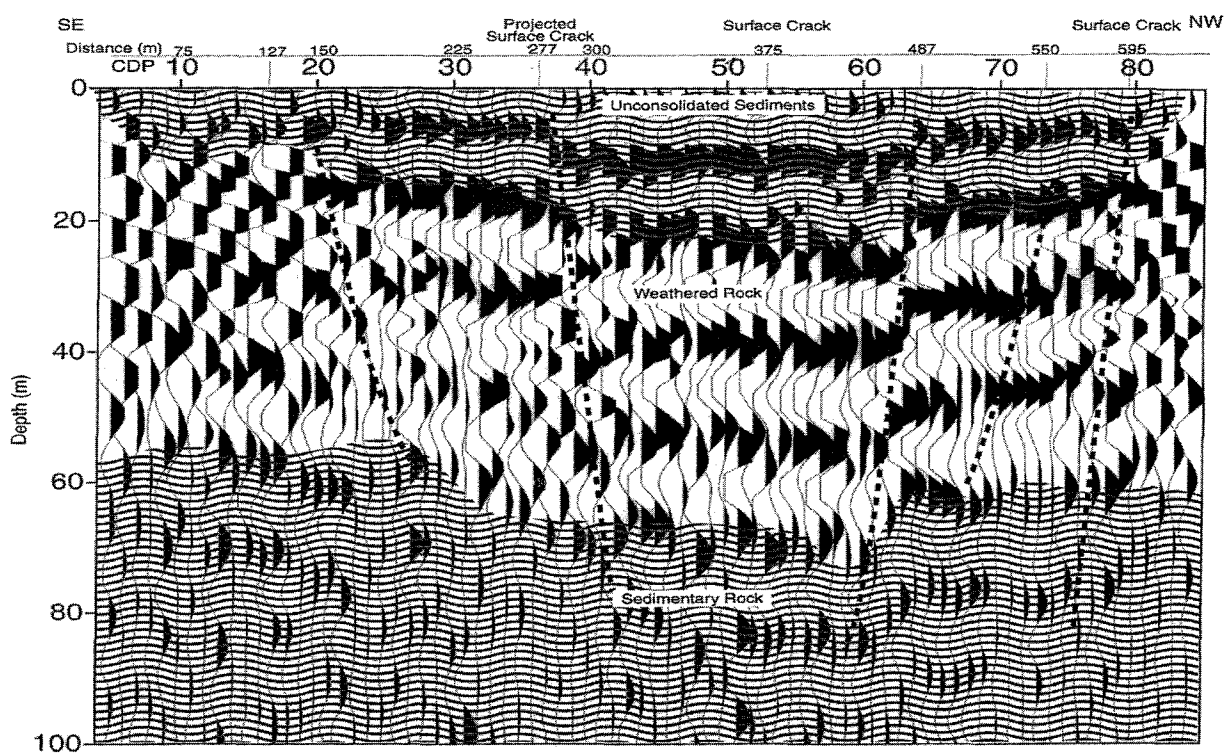

Figure 5. (a) Migrated seismic reflection section for the upper 100 m beneath the seismic array. Depth is relative to a datum equal to the topographically lowest point along the seismic profile. The horizontal axis is the common depth point (CDP) number, with the distance scale of the velocity model of Fig. 4 above the CDP numbers. Each CDP is approximately 7.5 m. The locations of surface cracks and a paleoseismological trench are shown along the top. (b) The seismic image from (a) with interpretative faults (dashed lines) and basic lithologic units.

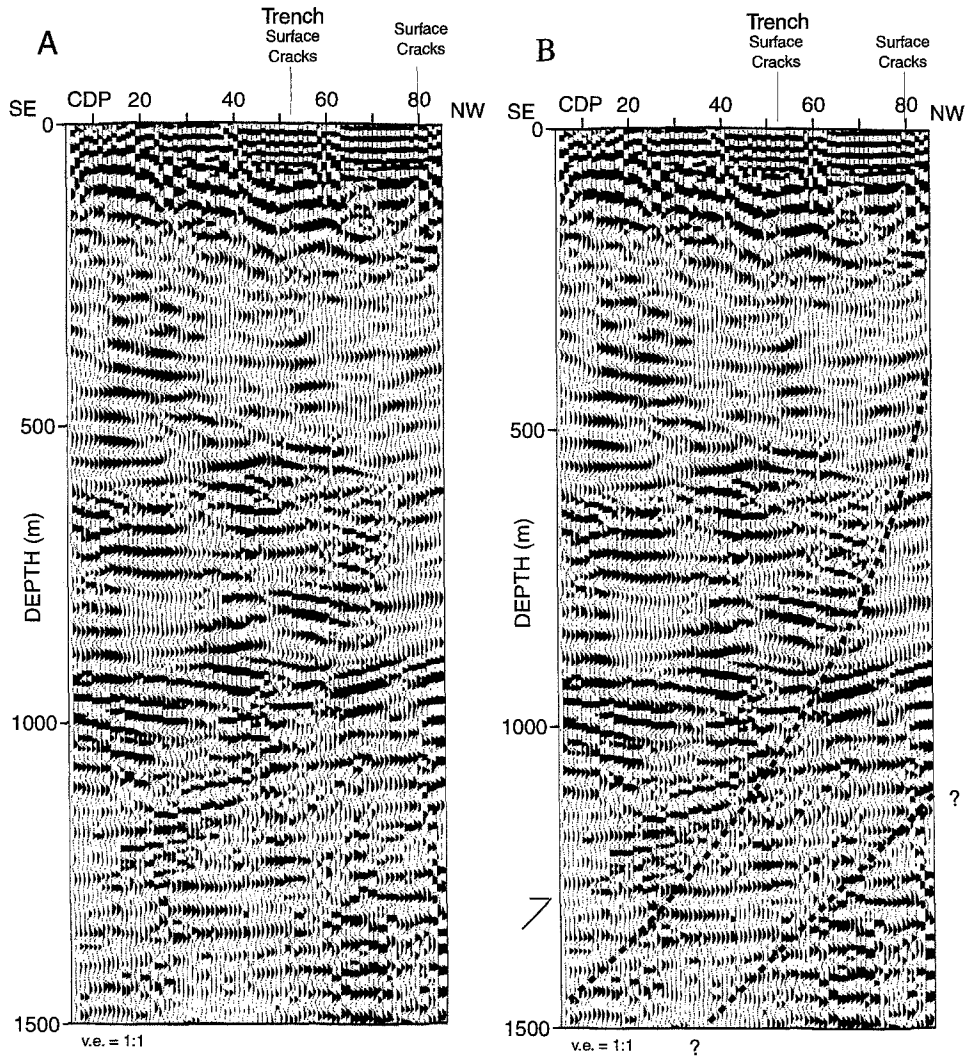

Figure 6. (a) Migrated seismic reflection section for the upper 1500 m beneath the seismic array, plotted as in Figure 5. (b) The seismic image from (a) with interpretative fault zones (dashed lines). The arrow points to an additional possible fault zone.

quake, but geodetic measurements are consistent with deeper (several kilometers) co-seismic movement in the vicinity of Potrero Canyon (Hudnut *et al.,* 1996; Shen *et al.,* 1996).

Deeper Subsurface and Faulting

We do not have seismic refraction measurements below 130 m depth due to the limited length of the seismic profile. Our characterization of the subsurface below about 130 m is derived from seismic reflection, geologic, and borehole data.

Relative to the upper 75 m, there are fewer reflectors from about 75 to 300 m depth, and the deeper reflections are lower in frequency, suggesting a change in lithology or physical condition (Fig. 6a). From about 300 m to about 600 m depth, the reflections are noticeably lower in amplitude than the overlying reflections, making it difficult to trace the near-surface faults in that depth range. However, the shallow faults appear to be truncated by underlying south-dipping reverse faults (Fig. 6b).

The seismic profile crosses Potrero Canyon at an angle of about 55°; therefore, imaged dips and structure are only apparent. However, in migrated seismic sections, Potrero Canyon appears to form a broad syncline (Fig. 6a) that is similar to the suggestion of Winterer and Durham (1962). The seismic section indicates that at shallow depths (<300 m), the steepest apparent dips of the reflectors (10° to 20°) are to the north, but at deeper depths (>500 m), the steepest apparent dips (~20°) are to the south. At about 1 km depth, these reflectors apparently dip gently (7°) to the north on the southern end of the seismic line and dip more steeply to the south (18°) on the northern end of the line (Fig. 6). However, these are minimum dips because of the angle at which the seismic line crosses structure.

The seismically observed variation in dips of the strata is greatest near apparent faults, such as the axial fault inferred by Winterer and Durham (1962) in Potrero Canyon (see Figs. 2 and 7). Similarly, geologic mapping along the southern end of the seismic profile (Winterer and Durham, 1962) and overturned bedding near the Oak Ridge fault on cross section 6b (Fig. 8a) of Yeats *et al.* (1994) also indicate high-angle stratigraphic dips near faults. These locally high dips may result from drag and rotation along reverse faults.

Although stratigraphic dips apparently vary appreciably in the area, fault dips appear to be predominately high angle. From about 600 m to 1 km depth, one or more reverse faults have apparent dips of about 50° to 60° to the southeast (Fig. 6b). However, because of the approximate 55° angle of our seismic line to the strike of Potrero Canyon, the true dip may be much more than the apparent dips, assuming that structure trends east–west. The short length of our seismic profile makes it difficult to verify, but there appears to be an additional fault imaged from about 1.1 to 1.5 km depth with a lower apparent dip of about 45°. Because these faults may have regional significance, we next explore some possible implications of the imaged faults.

Implications for Regional Fault Structure

Correlation of Seismic Image and Geologic Maps

The seismic images provide a continuous image of the upper 1.5 km for a distance of only about 700 m. This image, however, fills in a gap between existing well data and provides a two-dimensional view of faulting relationships that cannot be obtained from well data alone.

We interpret at least two deep fault zones in Figure 6b. The shallower of the two faults has an apparent dip between 50° and 60° and projects to the surface at a mapped syncline (Winterer and Durham, 1962; Yerkes and Campbell, 1995; see Fig. 7). To the west, the fold can be traced across the

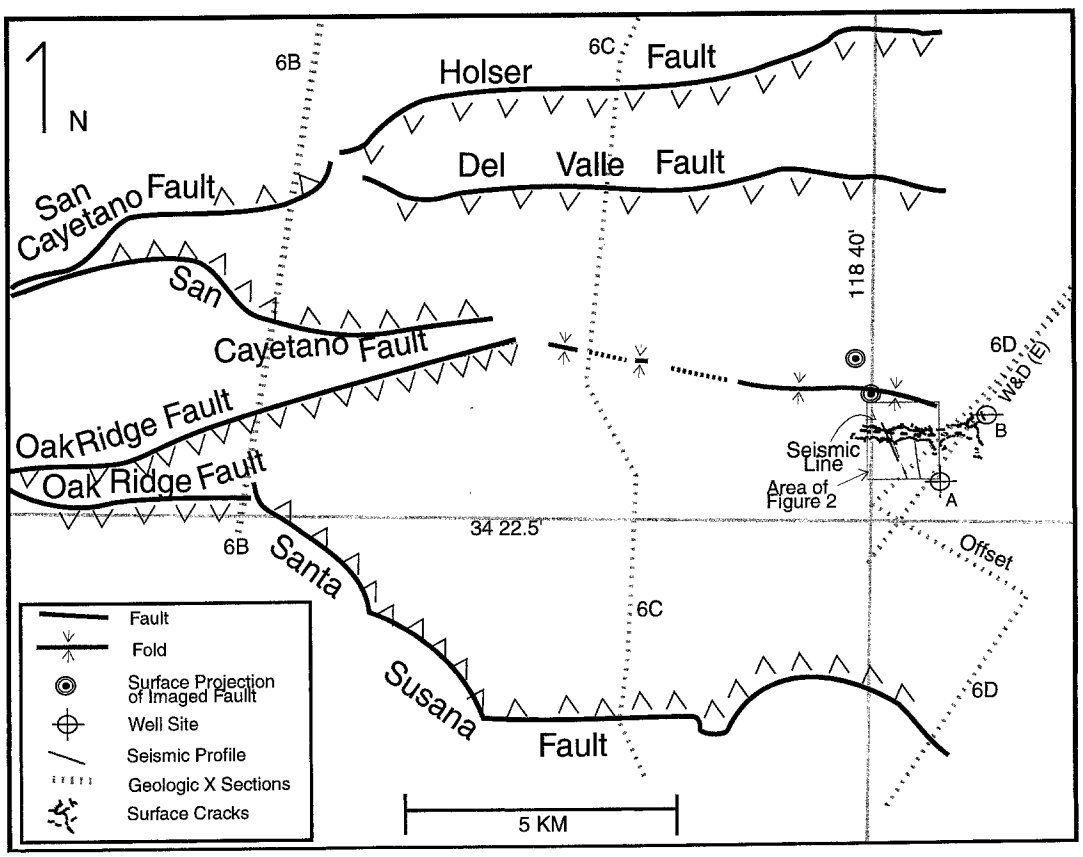

Figure 7. Location map of the major faults north of the Santa Susana mountains (from Yeats *et al.*, 1994). The fold shown extending east from the Oak Ridge fault is from the map of Yerkes and Campbell (1995). The box (light gray lines) shows the area of Figure 2. Within the box, the locations of our seismic profile, mapped surface cracks (from Rymer *et al.*, 1995), and an inferred axial fault by Winterer and Durham (1962) are shown. The circles north of the box indicate the approximate surface projection of the two deep (1.5 km) seismically imaged fault zones in Figure 6. The locations of geologic cross sections labeled W&D (see Fig. 9), 6b (see Fig. 8a), 6c (see Fig. 8b), and 6d (Fig. 8c) are shown relative to our seismic profile.

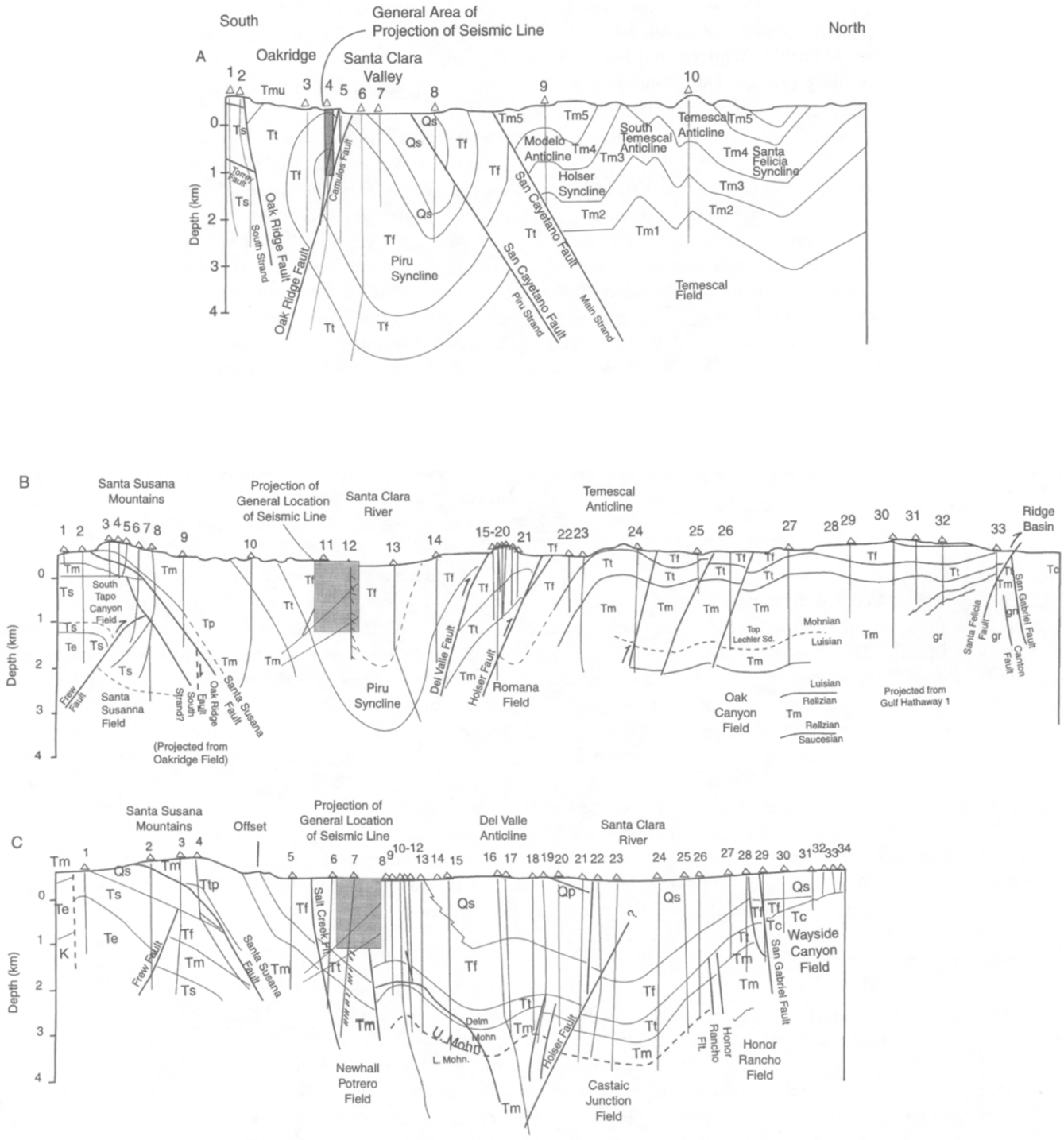

Figure 8. (a) Cross section 6b from Yeats *et al.* (1994) with a general-area projection of our seismic profile (gray box) at the approximate latitude of our seismic profile. Light gray lines with numbers above show the locations of wells. (b) Cross section 6c from Yeats *et al.* (1994) showing the general-area projection of our seismic profile. Dips are implied by the dipping lines on well 12. (c) Cross section 6d from Yeats *et al.* (1994) showing the general location of the projection of our seismic line. Depth ranges with dip-meter information on well 7 is shown. See Yeats *et al.* (1994) for explanation of the geology.

Santa Clara Valley toward the northern strand of the Oak Ridge fault (Fig. 7). The spatial relationship among the imaged fault, the fold, and the Oak Ridge fault suggests that the surface fold is the surface expression of or is related to the eastern continuation of the Oak Ridge fault; suggesting that the fault imaged in Figure 6 is a subsurface image of the Oak Ridge fault. This relationship implies that the Oak Ridge fault continues much farther east as a progressively deeper blind thrust fault.

Eastward of our seismic profile, the surficial fold associated with the Oak Ridge fault is apparently discontinuous at the surface at about the same longitude as the discontinuations of Holser and Del Valle faults. However, we suggest that the imaged fault becomes a more deeply buried fault along the eastward projection of the fold in a manner similar to east-southeast plunging folds associated with the Del Valle and Holser Faults to the north. The folds extending eastward from the Holser and Del Valle faults may also represent surficial expressions of blind thrust faults that continue to the east. This possibility is supported by cross sections drawn by Winterer and Durham (1962) and Yeats *et al.* (1994).

Correlation with Cross Sections Interpreted from Well Log Data

On the basis of well logs from deep oil wells in the area surrounding Potrero Canyon, the geology and structure of the area has been interpreted in cross sections by Winterer and Durham (1962) and Yeats *et al.* (1994). Cross section 6b (Fig. 8a) shows the structural setting and dip of the Oak Ridge fault to the west, where it is exposed at the surface. There, the Oak Ridge fault is segmented into two strands, a north strand and a south strand. On the basis of surface mapping and borehole data, Yeats *et al.* (1994) suggest a vertically discontinuous north-dipping south strand and a vertically continuous south-dipping north strand. This relationship suggests that the north strand cuts the south strand at depth (Fig. 8a). The north strand of the Oak Ridge fault surfaces on the south limb of the Santa Clara Valley syncline (Fig. 8a).

At the surface, bedrock strikes approximately east–west between our seismic profile and section 6b, and Potrero Canyon strikes approximately east–west (Winterer and Durham, 1962). Therefore, with an approximate due westward, our seismic profile can be projected onto their cross section 6b in the general vicinity of the north strand of the Oak Ridge fault (Figs. 7 and 8a). Projection of our seismic section over such a long distance may not be valid; however, the general faulting relationship in cross section 6b is similar to that inferred in the seismic section.

At cross section 6c of Yeats *et al.* (1994), approximately 5 km west of our seismic profile, the Oak Ridge fault is not exposed at the surface but likely continues as the fold and imaged fault discussed earlier. We have projected our seismic section northwestward onto cross section 6c such that the spatial relationship between the fold and the imaged fault is maintained. Although the dips observed in the seismic section would steepen due to the projection angle (35°), the seismic section is somewhat consistent with the borehole data (Fig. 8b). Although it may be coincidental, the dip-meter data (well 12) shows changes in dip at the approximate depth of the imaged fault that we infer to be the Oak Ridge fault.

Sections 6d (Fig. 8c) of Yeats *et al.* (1994) and E-E′ (Fig. 9) of Winterer and Durham (1962) cross the eastern end of Potrero Canyon about 1.5 km east of our seismic profile and are the closest cross sections to our seismic line; however, these cross sections trend at a high angle (~60°) to the trend of our seismic profile. Therefore, because of laterally varying structure and angles of projection, neither cross section is ideal for comparison with our seismic profile, but general features, such as the existence of faults, can be compared. Although a true projection is not possible, we show the general geographical area that the seismic image projects toward section 6d (Fig. 8c). Well 7 (Fig. 8c) is located in the general area of our projection of the seismic line and may have intersected a fault similar to the one imaged; however, it is not known if well 7 intersected such a fault because there is not dip-meter information within the depth range (1.5 km) of our seismic data.

Some features interpreted on cross section E-E′ by Winterer and Durham (1962) on the basis of well data compare favorably with our imaged section. The general synclinal nature of Potrero Canyon and the relatively low-angle dips at less than 900 m (~3000 ft) depth agree on the two sections. Winterer and Durham's (1962) geologic mapping and our seismic section both infer a valley axial fault (see Fig. 2 and the fault at meter 487 on Fig. 4b); however, Winterer and Durham (1962) do not show a Potrero Canyon axial fault in cross section E-E′ because they infer that such a fault discontinues before it crosses section E-E′ (Figs. 2 and 7). Near our seismic profile, the existence of an axial fault in Potrero Canyon is also supported by the truncation of the Salt Creek fault at the longitude of our seismic profile (Fig. 2).

If our deeper-imaged faults are projected an additional 1.1 km south-southeastward, they approximately coincide with a fault that Winterer and Durham (1962) interpreted on the basis of well data (well A, Figs. 3 and 7) at about 2550 m (~8400 ft below ground surface, Fig. 9). Winterer and Durham (1962) suggest that the fault encountered in the well is the Salt Creek fault, but we suggest that their interpretation is not conclusive due to the limited borehole and dip-meter data. It is, therefore, also possible that the fault encountered in well A is one of the faults imaged on our seismic section.

Because the Potrero Canyon axial fault apparently cuts the Salt Creek fault near the surface, dips southward in our seismic section (located at meter 487 in Fig. 4b), and appears to be cut by or soles into our deeper-imaged faults (Fig. 6b), we suggest that the deeper faults (inferred here to be the Oak Ridge fault) may also cut the Salt Creek fault and continue both southward and eastward as part of the Northridge fault.

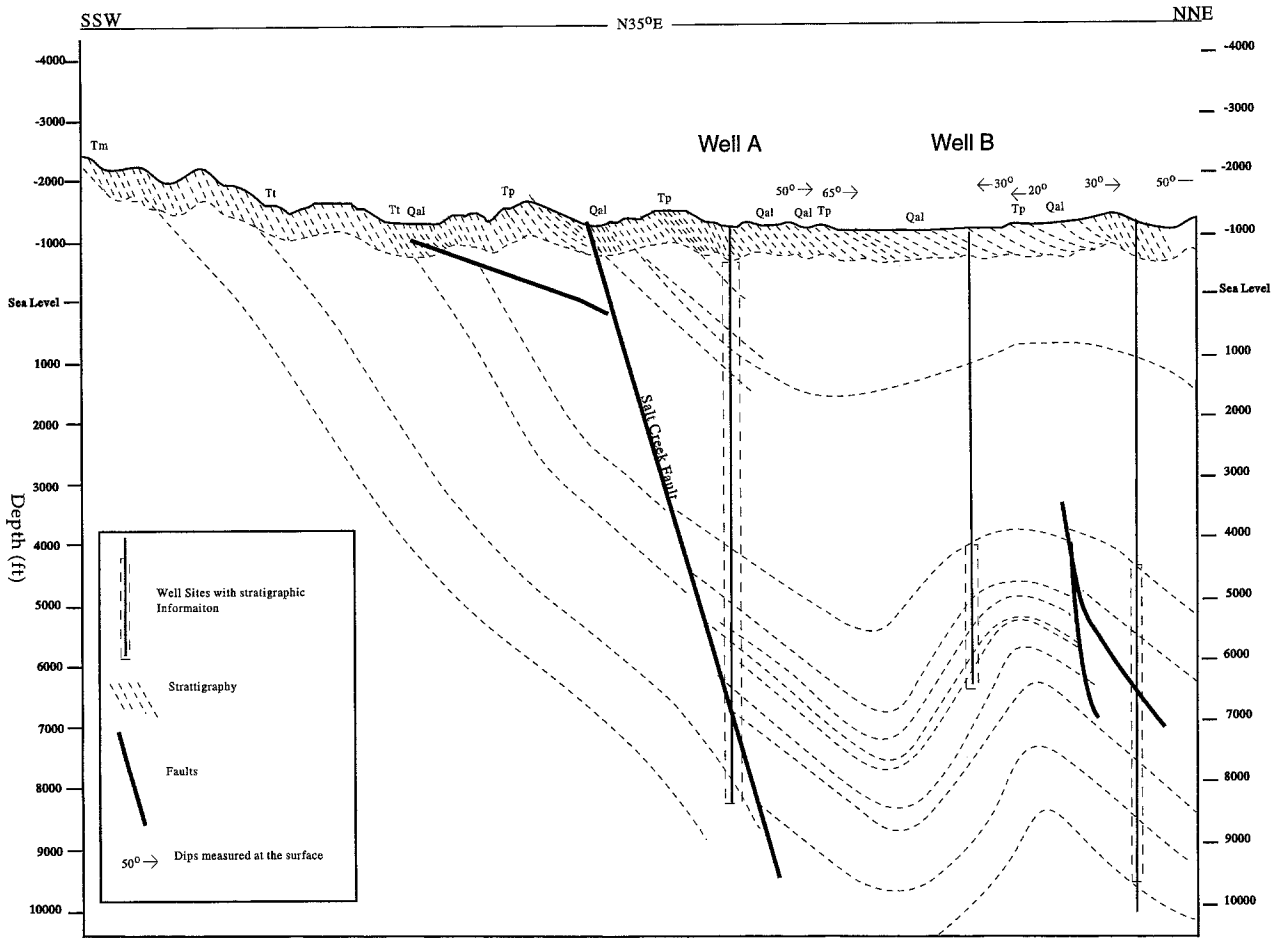

Figure 9. The southern part of cross section E-E′ by Winterer and Durham (1962). The southwestward projection of our imaged fault zones would intersect well A (see Fig. 7) near the approximate depth (2550 m; 8400 ft below ground surface) of a fault interpreted by Winterer and Durham (1962) to be the Salt Creek fault.

Implications of Combined Seismicity, Reflection, and Geologic Data

On the basis of seismicity data, geologic data, and well log data, Yeats and Huftile (1995) and Huftile and Yeats (1996) suggest that the Oak Ridge fault trends eastward from the approximate location of our seismic profile as a blind thrust and was the northern extension of the causative fault of the 1994 Northridge earthquake. Hauksson *et al.* (1995) suggest that the seismological data are consistent with the interpretation of Yeats and Huftile (1995) but suggest that the seismological data are consistent with other faults, including the Holser fault, as the causative fault.

Hauksson *et al.* (1995) show that the mainshock of the Northridge earthquake occurred on a fault plane that dips 35° to the south-southwest and strikes N75°W. They also show that a sequence of foreshocks and aftershocks outline a thrust ramp (from about 7 km to about 23 km depth) that is bounded by surficial faults, including the Santa Susana, San Cayetano, and Oak Ridge fault systems on the north and west. The dip of the ramp increases from east to west, whereby the west side of the ramp is characterized by a steeply dipping cluster of aftershocks with predominant thrust mechanisms. Schematic contours of the depth to the lower surface of the aftershock zone in the northwest appear to converge toward and northward of the Oak Ridge fault (Hauksson *et al.*, 1995), perhaps outlining the Oak Ridge fault as one of the causative faults. Although, at 3 to 13 km depth (Hauksson *et al.* 1995), the base of the thrust events projects westward toward the surface exposure of the Oak Ridge fault, the surface projection of these events would be north of the Oak Ridge fault, suggesting that other faults north of the Oak Ridge are involved.

We agree with Yeats and Huftile (1995) that the Oak Ridge fault is probably part of the causative fault system. However, on the basis of our seismically imaged fault patterns, the pattern inferred from cross sections by Yeats *et al.* (1994) and Winterer and Durham (1962), and seismicity data

(Pujol, 1996), we suggest that the Oak Ridge, Holser, Del Valle, as well as other south-dipping thrust faults between the Santa Susana mountains and the Holser fault may cut the north-dipping faults and join at depth into a single ramp that forms the causative fault of the Northridge earthquake.

Possible Seismic Reflection Artifacts

On the south end of the seismic profile, geologic mapping (Winterer and Durham, 1962; Rymer *et al.,* 1995) indicates that the stratigraphy dips steeply (65° to 70°) to the north. If the subsurface stratigraphy dips as much as 65°, the seismic reflection images in Figures 5 and 6 may be artifacts unrelated to primary layering. Apparent stratigraphy may be generated from out-of-the-plane reflections, reverberations from shallow layering, or secondary layering such as the water table. However, four lines of evidence argue against the imaged layers as artifacts.

First, the seismic refraction data show velocity anomalies at depths similar to those of the major series of reflectors. For example, near the center of the seismic profile, closely spaced velocity contours, which we interpret to be the bottom of unconsolidated sediments, are located at about 15 to 20 m depth (Fig. 4b). Similarly, an apparent reflection (Fig. 5b) is also located at about 15 to 20 m depth. A series of reflectors with varying dips and thicknesses are located between about 15 and 75 m depth. The base of this reflective sequence (Fig. 5b) correlates with the bottom of the closely spaced contours of the velocity model (Fig. 4b), consistent with the transition to more competent rock. Second, the seismic refraction data are an independent measure of the subsurface, and because only first arrivals are used in the inversion, out-of-the-plane reflections and reverberations do not affect the derived model. Thus, indications of similar faulting and stratigraphy in the same locations on both the velocity model (Fig. 4b) and the seismic image (Fig. 5b) argue strongly against the imaged features being artifacts. Third, if the imaged layers are related to out-of-the-plane reflections, they would likely arise from reflections off of the adjacent Salt Creek Fault (Fig. 2) or from the canyon walls. However, the Salt Creek Fault would generate only one reflection event, and the canyon walls would generate reflections whose travel times vary with the shot distance from the center of the valley. Multiples from the canyon walls would also produce a discrete time interval from each reflection. None of these observations are apparent in the seismic data. Fourth, the geologic and well data of Winterer and Durham (1962) indicate that the upper 1500 m (5000 ft) of stratigraphy (excluding the near surface on the south side of Potrero Canyon) should be relatively gently dipping (Fig. 9). Although we cannot be certain that the migrated seismic reflection images (Figs. 5 and 6) are not, in part, artifacts, most of the available geologic and geophysical data indicate that the images are primary reflections.

Discussion and Summary

The relative distance of Potrero Canyon from the Northridge earthquake epicenter and the rarity of other locations where surface cracks developed following the mainshock indicate that shaking at Potrero Canyon was unusually strong (D. Ponti and T. Holzer, unpublished map; Wald *et al.,* 1996). Gomberg (1997) suggests that dynamic strain measurements are consistent with the surface cracks developing from shaking alone; however, geodetic data and modeling (Hudnut *et al.,* 1996; Shen *et al.,* 1996) suggest that there was permanent deformation and likely co-seismic faulting in the deeper subsurface (several kilometers) in the Potrero Canyon area. Our seismic images show that at least two of the surface cracks in Potrero Canyon are underlain by apparent faults. Thus, we conclude the strong shaking and some of the resulting surface cracks in Potrero Canyon may have resulted from co-seismic movement on faults in the Potrero Canyon area. However, we cannot rule out other causes such as channeling of seismic energy along the faults, focusing of seismic waves as observed in the Santa Monica area (Gao *et al.,* 1996) and the San Francisco area during the 1989 Loma Prieta earthquake (Catchings and Kohler, 1996), or compaction along the faulted basin edge.

At depths greater than 0.5 km, there appear to be one or more reverse faults (fault zones), one of which is related to a fold at the surface and is spatially related to the Oak Ridge fault. If these faults continue east of our seismic line for appreciable distances, they apparently continue as buried or blind thrust or reverse faults. Our seismic image indicates that there is a general pattern whereby shallow, north-dipping faults are cut by the deeper south-dipping thrust or reverse faults. If such a faulting pattern persists throughout the study area, this seismically imaged faulting relationship, when combined with existing geologic, well log, and seismicity data, suggests that several south-dipping faults, bounded by the Santa Susana fault on the south and the Holser fault on the north, merge to form the causative fault zone of the 1994 Northridge earthquake.

Additional profiling of the type done in this study would be useful within the Santa Susana mountains and the Los Angeles County region to better define the faulting relationships and to better understand the earthquake hazard of the region. Because repeat times for fault systems are typically estimated on the basis of paleoseismological trenching studies, trenches that are mislocated or are located on only one strand of a multi-strand fault system can yield erroneous repeat times and magnitudes. In addition, hazard evaluations based solely on trenched surface faults do not include the hazard associated with blind thrust faults. Seismic imaging studies may identify these faults so that a more complete hazard assessment can be made. This type of combined reflection and refraction survey is particularly useful for hazard assessment because it also provides a measure of the seismic velocity and basin shape needed in engineering applications.

Acknowledgments

This investigation was funded by the U.S. Geological Survey's National Earthquake Hazard Reduction Program. David Harlow, Alexi Kolesnekov, Keith Rice, David Schwartz, and Randall White assisted in data acquisition. We thank Shane Detweilder, Gini Gandhok, T. Holzer, Chuck McGee, J. A. Treiman, and an anonymous reviewer for comments.

References

Catchings, R. D. and W. M. Kohler (1996). Reflected seismic waves and their effect on strong shaking during the 1989 Loma Prieta, California, earthquake, *Bull. Seism. Soc. Am.* **86,** 1401–1416.

Catchings, R. D. and W. H. K. Lee (1996). Shallow velocity structure and Poisson's ratio at the Tarzana, California, strong-motion accelerometer site, *Bull. Seism. Soc. Am.* **86,** 1704–1713.

Fumal, T. E., J. F. Gibbs, and E. F. Roth (1981). In-situ measurements of seismic velocity at 19 locations in the Los Angeles, California region, *U.S. Geol. Surv. Open-File Rept. 81–399,* 119 pp.

Gao, S. H. Liu, P. M. Davis, and L. Knopoff (1996). Localized amplification of seismic waves and correlation with damage due to the Northridge earthquake: evidence for focusing in Santa Monica, *Bull. Seism. Soc. Am.* **86,** S209–230.

Gomberg, J. (1997). Dynamic deformations and the M6.7 Northridge, California earthquake, *Soil Dyn. Earthquake Eng.* **16,** 471–494.

Hart, E. A., J. A. Treiman, and W. A. Bryant (1995). The search for fault rupture after the Northridge earthquake, in *Northridge, California Earthquake, January 17, 1994,* W. R. Seiple and M. Woods (Editors), *Calif. Div. Mines Geol. Spec. Publ.* **116,** 89–101.

Hauksson, E., L. M. Jones, and K. Hutton (1995). The 1994 Northridge earthquake sequence in California: seismological and tectonic aspects, *J. Geophys. Res.* **97,** 12335–12355.

Hecker, S., D. J. Ponti, C. D. Garvin, and J. C. Hamilton (1995). Characteristics and origin of ground deformation produced in Granada Hills and Mission Hills during the January 17, 1994 Northridge earthquake, in *Northridge, California Earthquake, January 17, 1994,* W. R. Seiple and M. Woods (Editors), *Calif. Div. Mines Geol. Spec. Publ.* **116,** 111–131.

Hole, J. A. (1992). Nonlinear high-resolution three-dimensional seismic travel time tomography, *J. Geophys. Res.* **97,** 6553–6562.

Holzer, Thomas L., M. J. Bennett, J. C. Tinsley III, Daniel J. Ponti, and Robert V. Sharp (1996). Causes of ground failure in alluvium during the Northridge, California, earthquake of January 17, 1994, in *U.S.–Japan Workshop on Earthquake Resistant Design of Lifeline Facilitates and Countermeasures against Liquefaction, 6th Tokyo 1996 Proceedings,* M. Hamada and T. D. O'Rourke (Editors), *Natl. Center Earthquake Eng. Res. Tech. Rept. NCEER-96-0012,* 345–360.

Hudnut, K. W., Z. Shen, M. Murray, S. McClusky, R. King, T. Herring, B. Hager, Y. Feng, P. Farg, A. Donnellan, and Y. Bock (1996). Coseismic displacements of the 1994 Northridge, California, earthquake, *Bull. Seism. Soc. Am.* **86,** S19–S36.

Huftile, G. J. and R. S. Yeats (1996). Deformation rates across the Placerita (Northridge M_w = 6.7 Aftershock Zone) and Hopper Canyon segments of the western Transverse range deformation belt, *Bull. Seism. Soc. Am.* **86,** S3–S18.

Jaasma, M. N., R. D. Catchings, M. J. Goldman, M. J. Rymer, and W. H. K. Lee (1997). Seismic reflection images and interpretation for seismic reflection data beneath Potrero Canyon, Los Angeles County, California, *U.S. Geol. Surv. Open-File Rept. 97–283,* 19 pp.

Jarchow, C. M., R. D. Catchings, and W. J. Lutter (1994). Large-explosive-source, wide-recording-aperture seismic profiling on the Columbia Plateau, Washington, *Geophysics* **59,** 259–271.

Lee, W. H. K. (Editor) (1989). Toolbox for seismic data acquisition, processing, and analysis, *IASPEI Software Library,* Vol. 1, Seis. Soc. Am., El Cerrito, California, 278 pp.

Lee, W. H. K. and D. A. Dodge (Editors) (1992). A course on: PC-based seismic networks, *U.S. Geol. Surv. Open-File Rept. 92–441,* 535 pp.

Lutter, W. J., R. D. Catchings, and C. M. Jarchow (1994). An image of the Columbia Plateau from inversion of high-resolution seismic data, *Geophysics* **59,** 1278–1289.

Pujol, J. (1996). An integrated 3D velocity inversion—joint hypocentral determination relocation analysis of events in the Northridge area, *Bull. Seism. Soc. Am.* **86,** S138–S155.

Rymer, M. J., T. E. Fumal, D. P. Schwartz, T. J. Powers, and F. R. Cinti (1995). Distribution and recurrence of surface fractures in Potrero Canyon associated with the 1994 Northridge, California, earthquake, in *The Northridge, California, Earthquake of 17 January 1994,* Mary C. Woods and W. Ray Seiple (Editors), *Calif. Depart. Conservation, Div. Mines Geol. Spec. Publ.* **116,** 133–146.

Shen, Z., B. X. Ge, D. D. Jackson, D. Potter, M. Cline, and L. Sung (1996). Northridge earthquake rupture models based on global positioning system measurements, *Bull. Seism. Soc. Am.* **86,** S37–S48.

U.S. Geological Survey and Southern California Earthquake Center (1994). The magnitude 6.7 Northridge, California, earthquake of 17 January 1994, *Science* **266,** 389–397.

Wald, D. J., T. H. Heaton, and K. W. Hudnut (1996). The slip history of the 1994 Northridge, California, earthquake determined from strong-motion, teleseismic, gps, and leveling data, *Bull. Seism. Soc. Am.* **86,** S49–S70.

Wentworth, C. M. and R. F. Yerkes (1971). Geologic setting and activity of faults in the San Fernando area, California, in *The San Fernando, California, Earthquake of February 9, 1971, U.S. Geol. Surv. Profess. Pap.* **733,** 6–16.

Winterer, E. L. and D. L. Durham (1962). Geology of southeastern Ventura basin, Los Angeles County, California, *U.S. Geol. Surv. Profess. Pap.* **334,** 275–366.

Yeats, R. S. and G. J. Huftile (1995). Oak Ridge fault system and the 1994 Northridge earthquake, *Nature* **373,** 418–420.

Yeats, R. S., G. J. Huftile, and L. T. Stitt (1994). Late Cenozoic tectonics of the east Ventura Basin, Transverse Ranges, California, *AAPG Bull.* **78,** 1040–1074.

Yerkes, R. F. and R. H. Campbell (1995). Preliminary geologic map of the Val Verde 7.5′ quadrangle, southern California, *U.S. Geol. Surv. Open-File Rept. 95–504,* 9 pp.

U.S. Geological Survey
345 Middlefield Rd. MS 977
Menlo Park, California 94025

Manuscript received 7 July 1997.